Mm-Wave Beam-Steerable Endfire Array Embedded in a Slotted Metal-Frame LTE Antenna

Rodriguez Cano, Rocio ; Zhang, Shuai; Zhao, Kun; Pedersen, Gert Frølund

Published in:
I E E E Transactions on Antennas and Propagation

DOI (link to publication from Publisher):
10.1109/TAP.2020.2963915

Publication date:
2020

Document Version
Accepted author manuscript, peer reviewed version

Mm-Wave Beam-Steerable Endfire Array Embedded in Slotted Metal-Frame LTE Antenna

Rocio Rodriguez-Cano, *Student Member, IEEE*, Shuai Zhang, *Senior Member, IEEE*, Kun Zhao and Gert Frølund Pedersen, *Member, IEEE*

***Abstract*—In this paper, a new principle to overcome the blockage of metallic frames in mobile terminals to endfire millimeter-wave (mm-wave) arrays is proposed. The obstruction is solved by etching several slots in the top part of the frame. It is shown that the slots in the handset frame can furthermore enhance the beam-steering gain of a mm-wave bow-tie array. A very small array-frame distance can also be realized without degrading much the array performance. Several considerations in the slot design are assessed first. A prototype of the PCB and frame has been built and the results show that the array is matched in the desired frequency bands of 24.25-27.5 GHz and 27.5-28.35 GHz. The mm-wave array can scan 80 degrees in the endfire direction, and the realized gain obtained is higher than 7 dBi in the operating frequency bands. At the same time, the frame performs as a sub-3 GHz dual-loop antenna. The covered bands are 760-980 MHz and 1240-2870 MHz.**

***Index Terms*—5G mobile communication, beam-steering, endfire, handset antennas, millimeter wave, phased array, slot antenna.**

I. Introduction

THE inclusion of the millimeter-wave (mm-wave) bands in the fifth generation of mobile communication (5G) spectrum, has prompted the appearance of higher gain antenna systems in mobile terminals [1]–[4]. Different antenna arrays have been proposed in the literature to cover the new frequency bands [5]–[11]. The increasing number of antennas in handsets provides challenges in terms of the inclusion of these new antennas.

The embedding of mm-wave antenna systems in antennas in the sub-6 GHz is a good solution for tight space constraints. Nevertheless, since the wavelength of the mm-wave array is smaller, the antennas are more sensitive to the blockage of any metallic structures placed nearby. In [12], the mm-wave array is embedded in a planar inverted F-antenna (PIFA) that covers the sub-3 GHz band. The solution proposed to prevent the obstruction from the PIFA on the mm-wave antenna is to add a layer of grating strips between the two antennas, at a distance of $\lambda/4$ from the PIFA, so that the reflections cancel out. However, this solution does not consider the metallic frame of the handsets, which is commonly used in the industry, but a planar structure. Two 4G monopoles have been embedded in a mm-wave slot array in [13], but the metallic frame is not considered in the design. In [14], a mm-wave antenna module is embedded in the metal rim of the handset, that is utilized as a LTE antenna. A 25 mm $\times$ 10 mm $\times$ 6 mm window is cut from the metal rim for the mm-wave module. Since the array is delimited by the metal frame, the beam-steering range is limited to $\pm 25^{\circ}$. In [15], a mm-wave array is embedded in a metal-frame antenna, which covers some of the sub-3 GHz bands. The beam can scan $\pm 60^{\circ}$, with a gain higher than 10 dBi in all the frequency range. Several solutions of slot arrays etched on the handset frame are proposed in [7], [16]–[18]. However, in these cases, the co-design of the metal-frame antenna and mm-wave array would become more complex, since the feeding networks of the mm-wave antenna have to connect the metal frame with the ground plane of the phone. This significantly changes the modes of the low-frequency antenna and thereby its performance.

In this paper, a dual-element phased array is proposed to cover the 5G bands n258 (24.25-27.5 GHz) and n261 (27.5-28.35 GHz) [19]. The proposed design presents a solution to overcome the frame blockage of horizontally-polarized endfire mm-wave antennas, that achieves high gain and large beam-steering range. The mm-wave array is embedded in a slotted-metal frame antenna, that enhances the gain of the 5G array. With higher gain, the number of driven antennas can be reduced, which decreases the complexity of the array, since fewer phase shifters and other components are needed. As the slots are fed by the electromagnetic coupling from mm-wave array to the frame, the complexity of the embedding in the low frequency antenna is significantly reduced. Simulations are carried out by CST Microwave Studio 2019. The novelty and contribution of this paper are summarized and listed as follows:

1) The co-design of the low-frequency and mm-wave antennas is simple after the embedding, which is because the slots in the frame are fed by the coupling of the mm-wave array.
2) Improvement of the mm-wave array gain after the embedding, which allows employing less active elements in the 5G mm-wave array.
3) The proposed concept is valid for very wide metal frames and small clearances. Moreover, the performance is robust to different antenna-frame distances.

The manuscript is organized as follows: the proposed design is specified in Section II. Section III describes the principle proposed to overcome the frame blockage to endfire mm-wave antennas. Design considerations are analyzed in Section IV to

This work was supported by the InnovationsFonden project of Reconfigurable Arrays for Next Generation Efficiency (RANGE).

Rocio Rodriguez-Cano, Shuai Zhang, Kun Zhao and Gert F. Pedersen are with the Antenna, Propagation and Millimeter-Wave Section (APMS) at the Department of Electronic Systems, Aalborg University, 9220 Aalborg, Denmark. Corresponding author Shuai Zhang (e-mail: sz@es.aau.dk).

Kun Zhao is also with Sony Research Center Lund, Sweden.

determine the final configuration, such as slot shape, number of slots, the separation between the slots, antenna-frame distance and number of active elements. The performance of the final design is shown in Section V. In Section VI, a comparison between the state of art and the solution proposed in this paper is presented. Finally, conclusions are given in Section VII.

II. Proposed Design

The proposed design consists of a mm-wave phased array embedded in a slotted metal-frame antenna that covers the sub-3 GHz bands. The antennas are represented in Fig. 1. The mm-wave antenna is etched on Rogers RO4350B substrate of thickness 0.254 mm, and dielectric permittivity of 3.48. The chosen geometry of the mm-wave array is a quad-element antipodal bow-tie array, with only 2 active elements, fed by coaxial cables. Bow-tie antenna elements have been selected since they present a wide impedance bandwidth [20]. The dummy elements located at both sides of the mm-wave array are grounded. Their function is to provide similar boundary conditions for the 2 active elements. They have been optimized to offer the highest endfire gain without degrading the impedance matching of the antenna. The metal frame encloses the PCB, with a thickness of 0.3 mm and overall dimensions of 128 mm $\times$ 69.6 mm $\times$ 7 mm. The design of the bezel antenna is based on [21], that provides small ground clearance as a result of the use of lumped components. The grounding point and feeding of the frame antenna are represented in Fig. 1(b). The metallic part of the PCB is separated 2 mm from the frame on the sides, 2.78 mm on the top and 5.22 mm on the bottom. The PCB ground distance to the frame (2.78 mm) is defined by the design of the low-frequency antenna. The distance from the top part of the mm-wave antenna to the frame is obtained in Sec. IV-D and has a value of 0.5 mm. The slots etched on the top part of the frame are represented in Fig. 1(c). The slots etched on the frame barely modify the performance of the low-frequency antenna. The design parameters of the bow-tie mm-wave array and the slots etched on the frame are listed in Table I.

TABLE I
Dimensions of the Bow-tie Array and the Slots Etched on the Metal Frame (Unit: mm)

Parameter	Value	Parameter	Value
l_b	1.33	l_s	5.80
w_b	0.33	w_s	0.50
d_b	2.00	h_d	2.32
l_{f1}	3.45	l_{d1}	1.75
l_{f2}	3.00	l_{d2}	1.40
l_{f3}	1.50	w_d	0.15
w_{f1}	0.22	w_{f2}	0.50

III. Operating Principle

Previous studies from the authors show that the radiation patterns of endfire mm-wave arrays with vertical polarization are barely influenced by the metallic frame. On the other hand, it is critical for arrays with horizontal polarization [15]. For that reason, the focus of this paper is on the reduction of the frame blockage for endfire arrays with horizontal polarization.

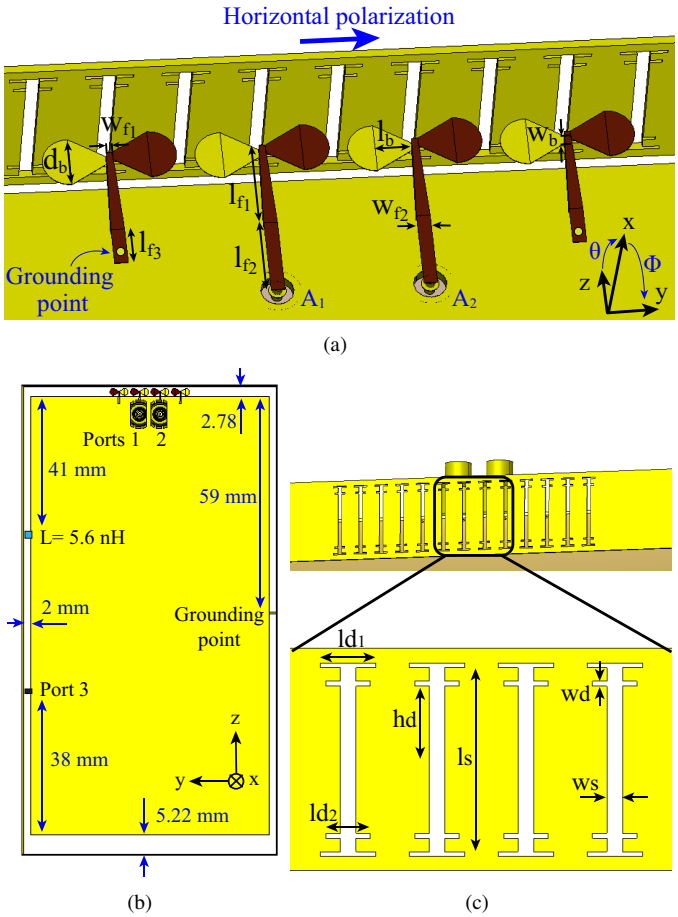

Fig. 1. Proposed embedded design. The substrate is delimited by the frame and is hidden in the figures. (a) Mm-wave array and top part of the frame with the slots etched. (b) Handset view. (c) Front view of the frame. Details of the slotted frame.

Please note that for convenience we refer to endfire direction as $+z$ axis, broadside as x axis, horizontal polarization with the E-field amplitude varying in the direction of the y axis and vertical polarization, in the direction of the x axis. The coordinate system can be found in Fig. 1(a).

As detailed in Section II, the proposed mm-wave array is composed of two end-fire antipodal bow-tie elements and two grounded dummy elements on the sides [see Fig. 1(a)]. Since the mm-wave antenna array has horizontal polarization, it excites horizontal currents on the frame, as shown in Fig. 2(a) and the radiation pattern is degraded. The resulting radiation pattern is mainly broadside, instead of endfire [Fig. 3]. In Fig. 2(a) the surface currents created by the antenna on the frame are represented. Therefore, if vertical slots are etched on the frame [see Fig. 1(c)], they would be fed by these currents and allow the mm-wave array radiate in the desired direction. The surface currents for the slotted frame are plotted in Fig. 2(b). It can be seen that the current concentration is higher around the slots. To demonstrate that the array is radiating in the correct direction, Fig. 3 shows the in-phase radiation pattern at the $\Phi = 0°$ cut of the array. This figure represents the impact of the frame on conventional endfire antennas with horizontal polarization. IEEE gain is plotted to exclude the mismatching loss of the different structures. It is defined as the antenna

directivity plus the radiation efficiency (in logarithmic scale). When there is no frame placed in front of the antenna, the main lobe of the array points to the endfire direction, with a value of 6.5 dBi. In the presence of the frame, the radiation pattern becomes broadside, with gain in the endfire direction of -5 dBi. For that reason, it is crucial to consider the impact of the frame in the design of horizontally polarized endfire mm-wave antennas. The radiation pattern of the solution presented in this paper also appears in Fig. 3. The slots etched on the top part of the frame not only overcome the blockage but make the radiation pattern to be more directive, with a gain of 7.7 dBi. The reason the main beam becomes more directive can be better understood by plotting the E-field. The instantaneous E-field in a longitudinal cut is represented in Fig. 4. When no frame is blocking the main beam of the array, the field distribution is larger around the mm-wave array. The wavefront propagates in the direction of the $+z$ axis. In the case of the unmodified frame, i.e, no slots [Fig. 4(b)], it can be seen that the electric field is blocked by the frame and the wavefront is propagating backward ($-z$ axis). However, the slots etched on the frame re-radiate the coupled energy from the bow-tie antenna, which increases the antenna aperture and leads to higher gain. Therefore, the E-field increases in the endfire direction [see Fig. 4(c)] and the wavefront is more directive than the case with no frame. The proposed solution can also be identified as the diffraction of curved wavefront on a metal frame with multiple slits. Since the mm-wave array is located 0.5 mm away from the frame, it corresponds to the Fresnel regime.

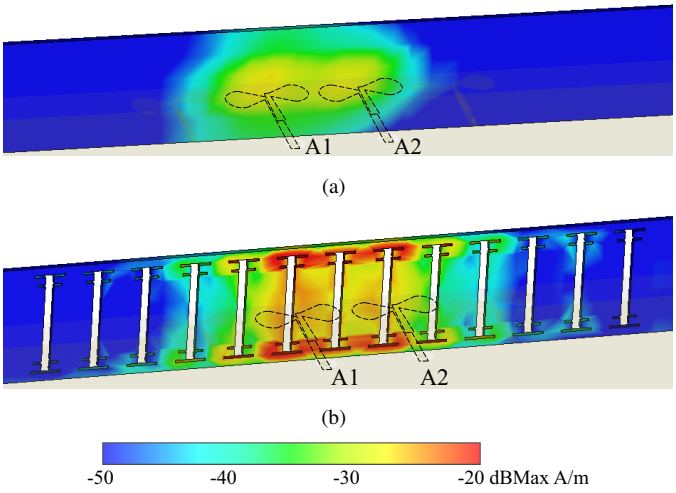

Fig. 2. Surface current on the top frame for the in-phase combination at 26 GHz. (a) No slots. (b) With slots.

IV. Design Considerations

In order to reveal the critical design parameters and demonstrate the robustness of the proposed design with different design scenarios, some configurations are assessed in this section. The considered parameters are the slot shape, number of slots, separation between the slots, antenna-frame distance and number of active elements. Since some of the parameters

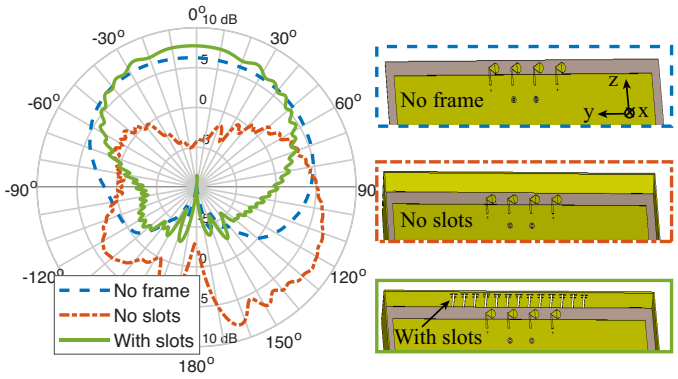

Fig. 3. IEEE gain radiation pattern of the in-phase array combination at 26 GHz for the $\Phi = 0^\circ$ cut.

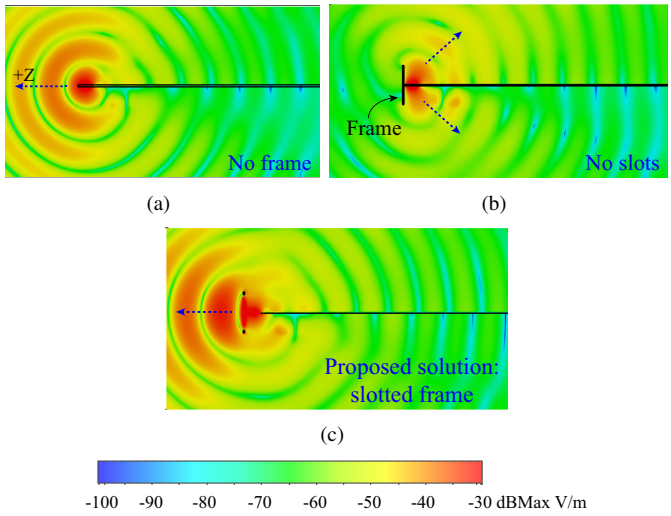

Fig. 4. Instantaneous E-field distribution cut in the XZ plane of the in-phase combination at 26 GHz. (a) No frame. (b) No slots. (c) With slots.

in the studies may change the impedance matching of the array, IEEE gain is represented to exclude the mismatch losses.

A. Effect of the slot shape

As described in Section III, horizontal currents are excited on the frame by the mm-wave antenna. Therefore, in order to couple with the horizontal polarized E-field and re-radiate it, vertical slots are etched on the frame. To maximize the gain out of the mm-wave array in the frequency bands, the dimensions of the slots need to be assessed. The length of the slot determines the resonant frequency. To obtain the optimum result, the resonant frequency of the slot should be in the middle of the frequency range of the antenna array. However, the width of the frame is a constraint, in this case, a value of 7 mm is chosen to adapt it to the width of the current terminals. For that reason, the slot cannot be enlarged progressively in a straight line and a dumbbell shape has been adopted [see Fig. 5]. As shown in the figure, the shape referred to as double dumbbell can further increase the gain of the array in the desired frequency bands and has been chosen for the final design. Fig. 6 shows the radiation pattern comparison at 1.5 GHz between the different slot shapes and no slots on the

frame. It can be seen that the slot shape has very limited impact on the performance of the LTE antenna.

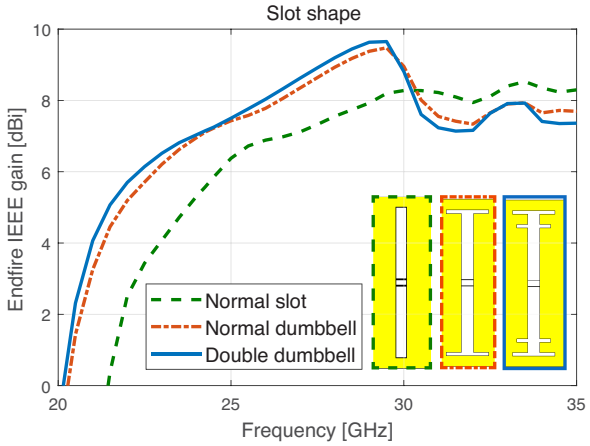

Fig. 5. IEEE gain in the endfire direction according to the slot shape.

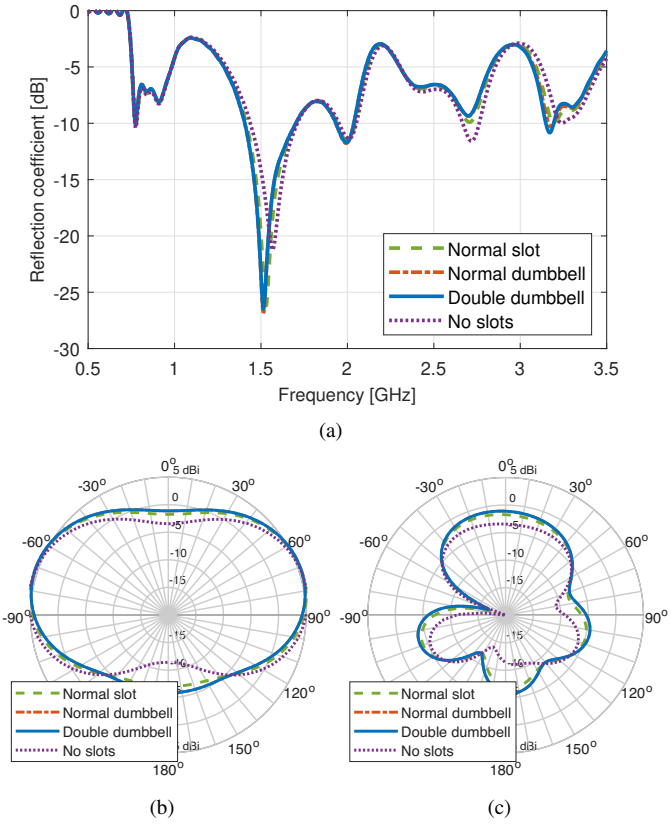

Fig. 6. Effect of the slot shape in the S parameters and the radiation pattern of the metal-frame antenna at 1.5 GHz. (a) Reflection coefficient. (b) Radiation pattern at $\Phi = 0^\circ$ cut. (c) Radiation pattern at $\Phi = 90^\circ$.

B. Number of slots

The number of slots etched on the frame has a strong impact on the gain in the endfire direction, as it can be seen in Fig. 7(a). The focus in this subsection corresponds to the design with two active elements and two dummy elements. The number of slots could straightforwardly be increased if more active elements are employed. In the case of 9 slots, the aperture of the slot array is the same as the mm-wave array. The gain of the mm-wave array without frame has been plotted as a reference, and the configuration with only 5 slots can already improve that performance. The gain in the endfire direction does not differ much when the number of slots is 7 or higher, but the radiation pattern becomes broadside when no slots are etched on the frame, as shown in Fig. 7(b). In terms of impedance mismatching, the configuration with frame with no slots is mismatched in all the operating bandwidth, since the majority of the radiation reflects back to the antenna. From 5 slots onward, the mm-wave array is matched below -10 dB from 24 to 29 GHz. In order to determine the number of slots which provides the best performance, the gain has also been plotted as a function of the beam-steering angle in Fig. 7(c). The figure provides the beam-steering envelope of a total of 12 beams. The phase step applied to get the different beams is 30°. The number of slots is also a critical parameter to achieve high beam-steering gain owing to the fact that, if the main beam points towards a place on the frame with no slots, the radiation would reflect back. Besides, it is important to have high gain with small variations between the beams pointing to different angles to reduce the complexity of the system. Moreover, high gain antennas have narrow beams, which are steered to cover the upper part of the sphere. Therefore, to determine the number of etched slots, it is necessary to consider the maximum beam-steering angle. The beam-steering envelope of these configurations is represented in Fig. 7(c) at 24.25 GHz, as the lower frequency band is the most sensitive. If only 9 slots are etched on the metal frame, the gain envelope is only higher than 7 dBi for $\theta = \pm 20^\circ$ at 24.25 GHz. This is due to a not large enough slot aperture. When 13 slots are added, the gain envelope is flatter, with a beam-steering range of $\pm 40^\circ$. For 15 slots, the scanning range could be enlarged, but with a gain lower than 7 dBi, which is the target. The configuration chosen for the final design is the one with 13 slots.

C. Separation between the slots

The separation between the slots is essential to maximize the radiated gain. The main beam of the antenna has endfire direction, hence the maximum value of the current excited on the frame is aligned with the center of the antenna, as shown in Fig. 2(a). For that reason, the separation of the slots depends on the separation between antenna elements (sep), which corresponds to $0.486\lambda_0$. The performance of several configurations is represented in Fig. 8. In the case of $0.375 \times sep$ ($0.182\lambda_0$) a distance of only 0.35 mm separates the slots from touching each other. The reflection coefficient shows that the antenna array is only matched when the separation between the slots is smaller than $0.5 \times sep$ ($0.243\lambda_0$). This configuration corresponds to having slots aligned with the center of every antenna and also in between the antenna elements, as shown in Fig. 8 (a). The separation between the slots is frequency dependent. The closer the separation between the slots, the easier higher frequencies (small wavelengths) propagate through

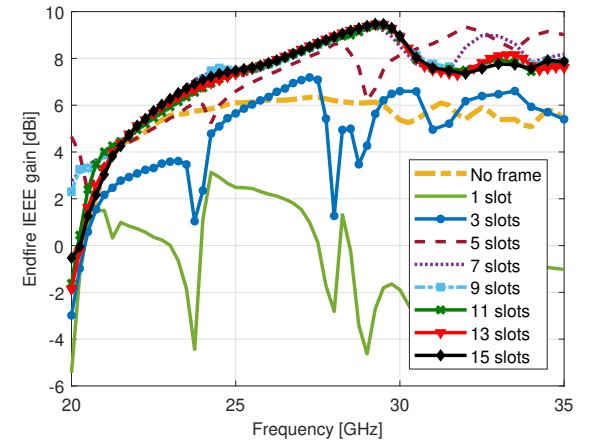

(a)

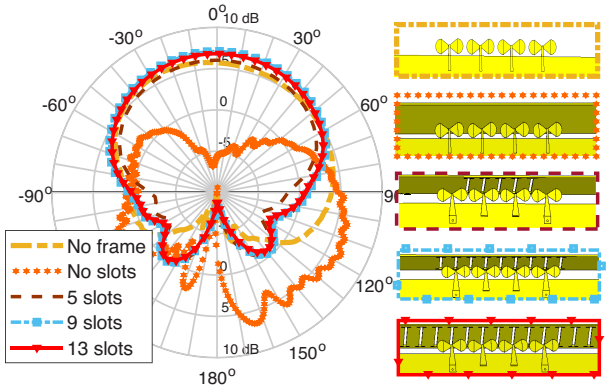

(b)

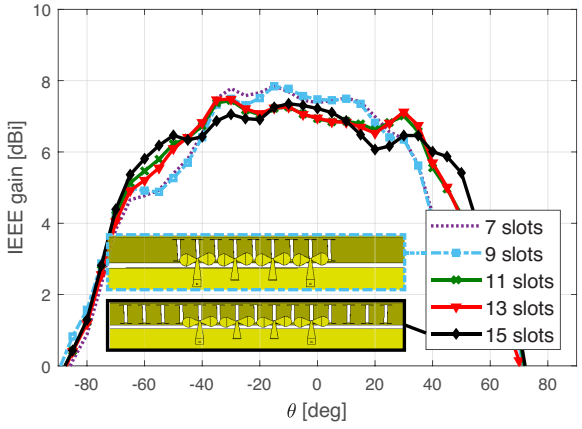

(c)

Fig. 7. (a) IEEE gain as a function of the frequency depending on the number of slots etched on the frame. The gain of the array with no frame is also compared. (b) IEEE gain radiation pattern at 24.25 GHz for $\Phi = 0°$ cut. (c) IEEE gain beam-steering envelope at 24.25 GHz.

the frame. As the separation between the slots increases, the endfire gain curve shifts to lower frequencies. In some of the larger separations, the gain can reach higher values but not throughout the whole frequency range and, besides, the impedance matching does not fulfill the expected -10 dB criterion. The value that provides an endfire gain of more than 7 dBi throughout the frequency band and a good impedance matching is $0.5 \times sep$ $(0.243\lambda_0)$.

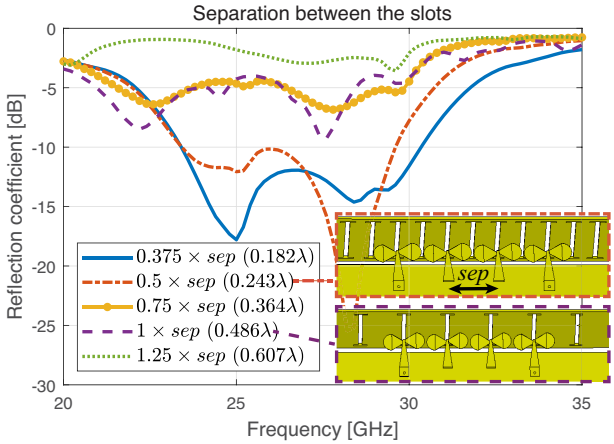

(a)

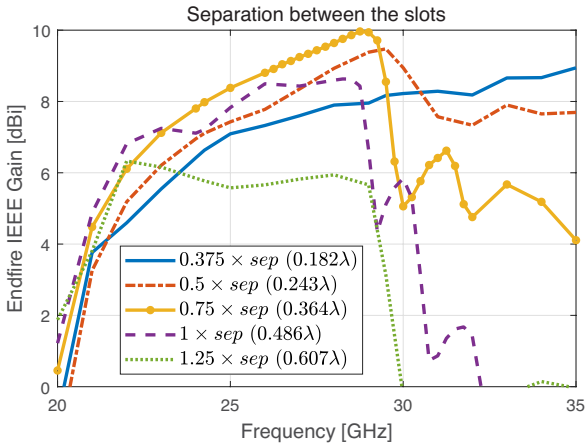

(b)

Fig. 8. Effect of the separation between the slots. (a) Reflection coefficient. (b) IEEE gain in the endfire direction.

D. Antenna array-frame distance

In order to illuminate the slots etched on the frame, the distance from the top of the antenna to the frame needs to be small. However, the closer the antenna is located to the frame, the more radiation would be reflected. In Fig. 9, the reflection coefficient and the IEEE gain in the endfire direction are represented. The gain maximum shifts to lower frequencies when the distance to the frame is enlarged. As the distance to the frame gets larger, the gain increases in the lower part of the frequency band but the impedance bandwidth is reduced. Due to this trade-off, a distance to the frame of 0.5 mm has been chosen for the final design. Even though there are variations in the results, the overall performance is very robust to the antenna-frame distance, which is an advantage in the fabrication process.

E. Number of active elements

At the 3GPP TR 38.817-01 specification for UE RF aspects in new radio (NR) [19], the minimum effective isotropic radiated power (EIRP) requirements for handsets (power class

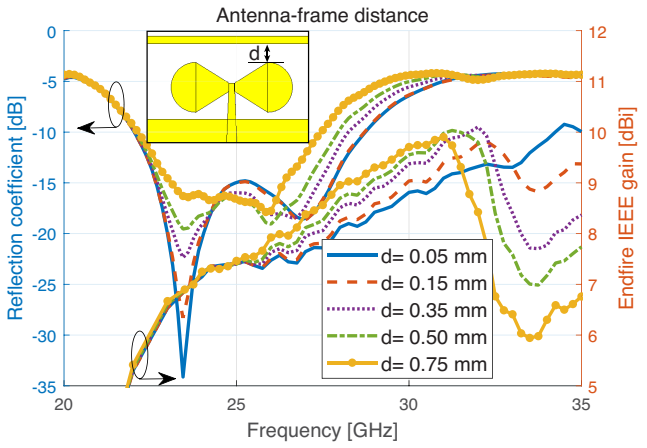

Fig. 9. Effect of the distance of the antenna to the frame, for both reflection coefficient and IEEE gain in the endfire direction.

3) in the mm-wave bands are based on an assumption of 4 active elements antenna arrays. This does not mean that the mm-wave arrays for terminals are required to have 4 elements, but gives an estimation of the number of antennas that are feasible to meet the minimum power required. Therefore, if an array with less active antennas can meet the requirements, it will be beneficial to reduce the size of the front-end module.

In this subsection, the advantages and disadvantages of adding two more active elements to the design are discussed. The design presented throughout the paper corresponds to 4 elements: 2 active and 2 dummy. As the slotted frame design can improve the array gain, it provides an opportunity to reduce the number of active elements. The idea is to compare it with the design of 4 antennas: 4 active elements without frame, since the gain achieved is similar. From the array point of view, two more elements provide higher gain and wider scanning range. The beam-steering envelope at 26 GHz is plotted in Fig. 10, with a gain increase of around 0.5 dB. From the front-end point of view, doubling the number of antennas would increase the complexity and cost of the system. On the other hand, the array gain would be further increased by double the number of elements and the power requirements of each antenna branch would be lower. If the power on the branch can be lower, the specifications of the power amplifier would be more relaxed, increasing the number of choices in the semiconductor technologies [22]. The 5G evaluation requirement for antenna arrays is defined as the EIRP spherical coverage (for the frequency range 2) [19]. The EIRP depends on two factors: the array antenna gain and the total radiated power. Even though the proposed design uses a smaller number of antenna ports, it can actually increase the antenna gain of the array after the embedding in the slotted-frame. For that reason, the overall array gain is not affected dramatically in the end, as represented in Fig. 10. On the other hand, the total radiated power can be affected due to the smaller number of antenna ports. The reason is that one of the most common architectures in mm-wave consists of having a power amplifier (PA) connected to each antenna port. Therefore, the number of power amplifiers might be reduced with a smaller number of antenna ports. Such RF architecture allows low-power and low-cost design of PAs to be used for handsets, for example, a CMOS type of PA [23]. One way to address this issue is to use a higher output power PA when the number of antenna ports is reduced, e.g. III-V type semiconductor PA, which could offer a higher output power and leverage total radiated power. Therefore, the number of elements will depend on the design of the whole front-end, but our proposed method provides an opportunity to reduce the number of antenna elements with a certain EIRP target.

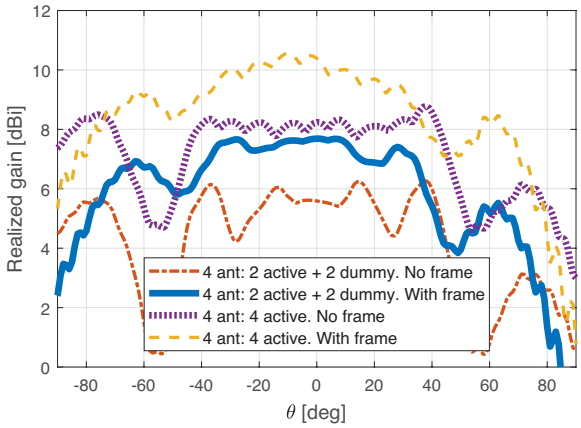

Fig. 10. Simulated beam-steering realized gain envelope comparison of the 2- and 4-element arrays with and without slotted frame at 26 GHz.

V. Results and Discussions

A prototype of the designed antenna has been fabricated to verify the simulation results. The dielectric tabs, that can be seen in Fig. 11 coming out of the frame, are made to hold the PCB in place, at the center of the frame. Their length and width are optimized to not interfere with the beam in the directions of maximum scan angle. A comparison between the measurements and simulations is assessed in the next paragraphs.

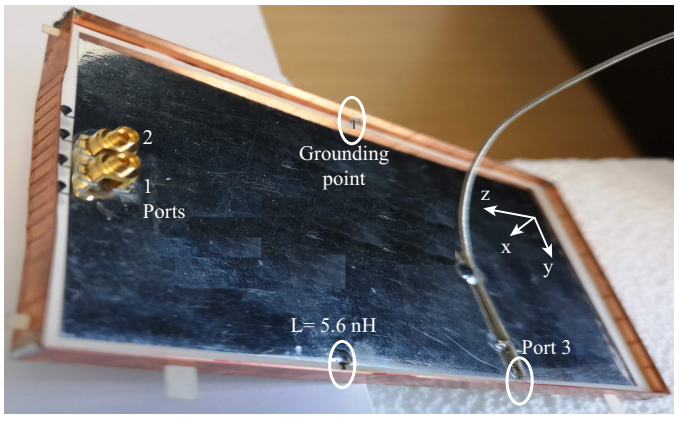

Fig. 11. Antenna prototype.

The reflection and transmission coefficients of the simulated and measured mm-wave array are plotted in Fig. 12(a). Good agreement can be found between measurements and

simulations. The bow-tie array is matched from 22 GHz to 28.4 GHz with -10 dB specification, which is more than enough to cover the 5G bands n258 (24.25-27.5 GHz) and n261 (27.5-28.35 GHz) [19]. The transmission coefficient is below -10 dB in the whole impedance bandwidth and below -15 dB in the bands of n258 and n261. The total efficiency of the mm-wave array is 92 %. The reflection coefficient of the frame antenna is represented in Fig. 12(b). For the sub-3 GHz antenna, the matching criterion is more relaxed and set to -6 dB. The measured antenna is matched at the frequency bands 760-980 MHz and 1240-2870 MHz. The total efficiency of the frame antenna is 77 % (760-980 MHz band), 90 % (1240-2090 MHz band) and 80 % (2355-2870 MHz band). It is important to guarantee that the low and high-frequency antennas are not going to modify their performance when they are simultaneously operated. The simulated mutual coupling between the frame antenna and the mm-wave array is below -15 dB in the low band and below -25 dB in the operating mm-wave band, as it is shown in Fig. 12.

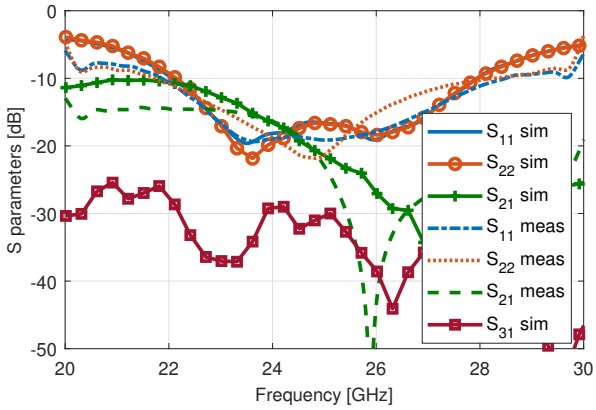

(a)

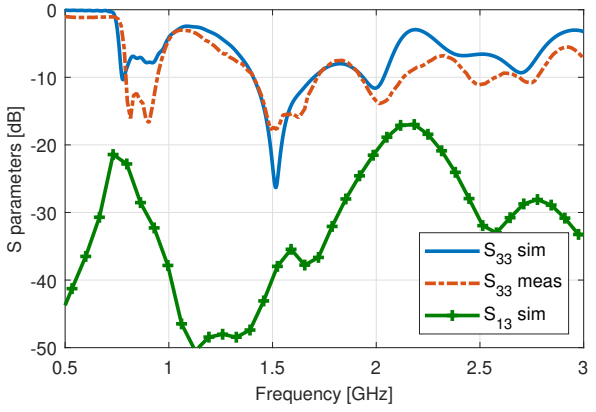

(b)

Fig. 12. Comparison of s-parameters between measurements and simulations. (a) Mm-wave array. (b) Sub-3 GHz antenna.

The measuring set-up of the anechoic chamber for the mm-wave array is shown in Fig. 13. Due to its configuration, θ values larger than 135° have been not plotted in the measured results [Fig. 13(b)]. The radiation patterns of the two antennas [numbering specified in Fig. 11] are plotted in Fig. 14 for the $\Phi = 0°$ cut and in Fig. 15, for the $\Phi = 90°$ cut. The simulated results are in a good agreement with the measurements at both 24 and 26 GHz. The radiation patterns point to the endfire direction and the measured gain is similar to the one obtained in the simulations, which means that the slots have successfully improved the gain of the mm-wave array.

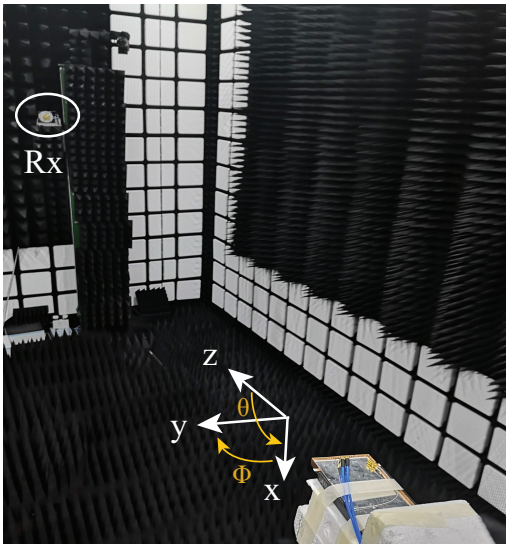

(a)

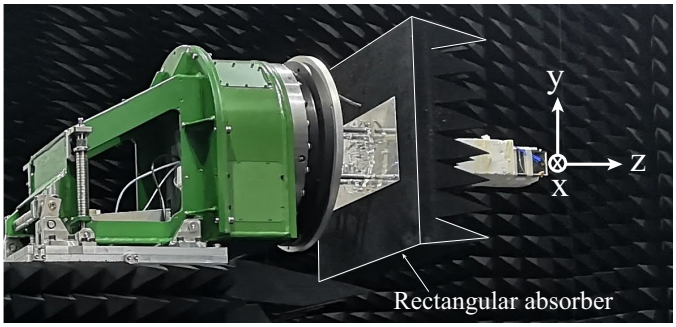

(b)

Fig. 13. Anechoic chamber set-up. (a) Transmitter and receiver. (b) Details of the mechanic arm.

The evaluation of the realized gain in the endfire direction as a function of the frequency is represented in Fig. 16. The combined gain, when the array is excited in phase, is higher than 7 dBi in the whole frequency range. Fig. 17 shows the beam-steering envelope comparison of the mm-wave array without frame and with a slotted frame at 24 and 26 GHz. The slots enhance the gain radiated from the antennas around 1 dB in the endfire direction and extend the scanning angle. When the bow-tie antenna points to the maximum scanning angle, the radiation pattern presents several ripples. However, scanning with the slotted frame helps to focus the energy in a certain direction and therefore, reduce the ripples. For that reason, the beam-steering envelope is flatter and broader when the slotted frame is placed in front of the antenna. The impact of the slotted-frame on the main beam direction has also been examined. Fig. 18 shows the effect of the frame for three different beams. The phase shifting between the two elements is $\Delta\varphi = 90°$, $0°$ and $-90°$, respectively. It can be

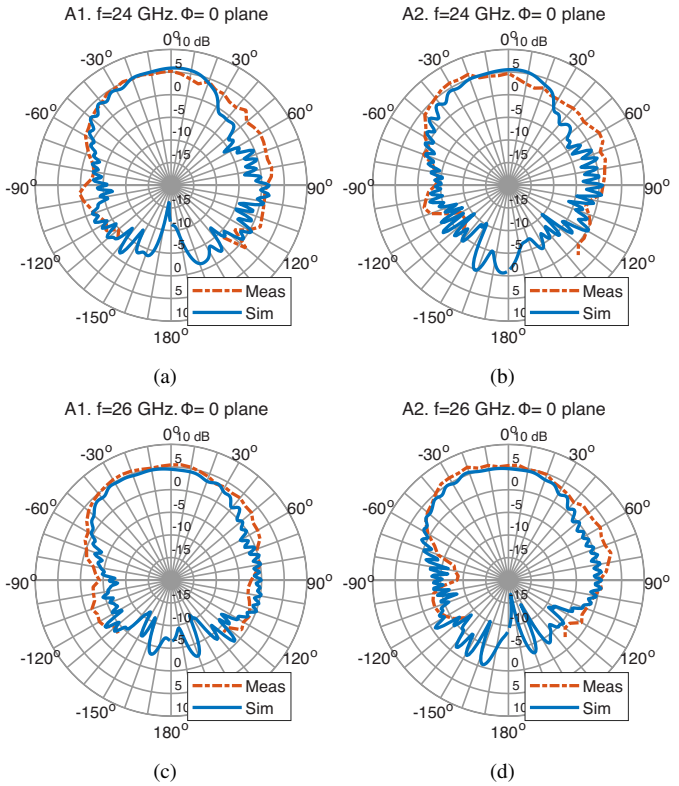

Fig. 14. Radiation patterns of the two active antennas at the $\Phi = 0^\circ$ at 24 and 26 GHz.

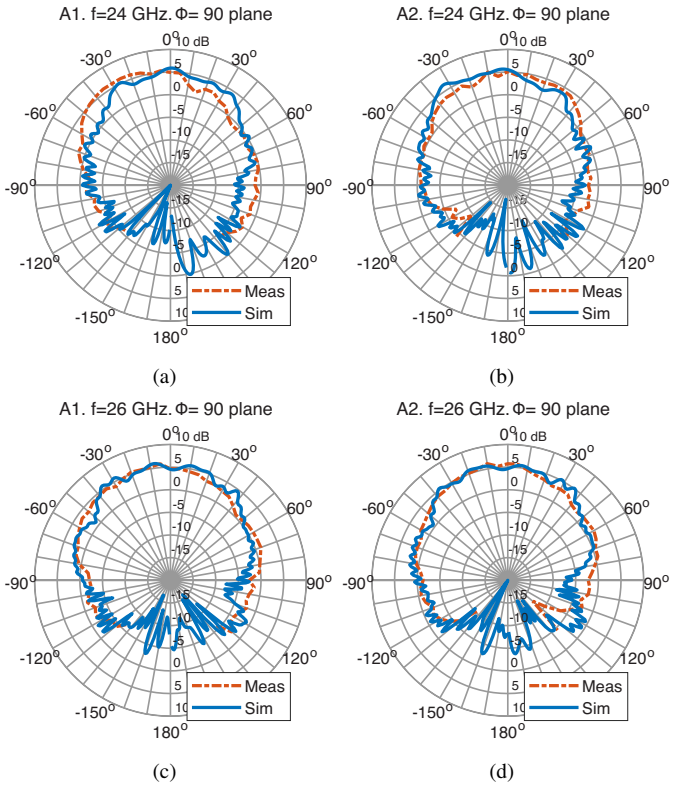

Fig. 15. Radiation patterns of the two active antennas in the $\Phi = 90^\circ$ at 24 and 26 GHz.

observed that, when the slotted-frame is added, the ripples are reduced and the beam gain is enhanced. The main beam remains towards similar directions with and without the metal frame. Therefore, the embedded array in the slotted metal-frame does not cause a significant error on beam alignment processes.

VI. Comparison with the State of Art

This contribution is compared with the state of art. The figures-of-merit (FoM) of all the proposed solutions are compared in Table II. Among the FoM, the term "embeddable" refers to the possibility of embedding the proposed mm-wave array in a sub-3 GHz frame antenna. The term "gain improvement" considers if there has been a gain enhancement in the mm-wave array after the embedding. The majority of the commercial handsets have a metallic frame. For that reason, the frame has been used as a location to place the mm-wave arrays in [7], [16], [17]. These designs use 8 active elements for the array, so the peak gain obtained is, in general, higher than in the other configurations. Nevertheless, the number of phase-shifters and power amplifiers increases and the remaining space in terminals is limited. Besides, the overall performance of these arrays is similar to the solutions with fewer elements. The embedding of a mm-wave array in a sub-3 GHz frame antenna has only been published in a few papers [14], [15], [18] to the best of the authors' knowledge. Even though the number of active elements is bigger than 4 in [14], [18], the beam-steering range of both proposals is lower than 60°, which would force the handset to have 4 mm-

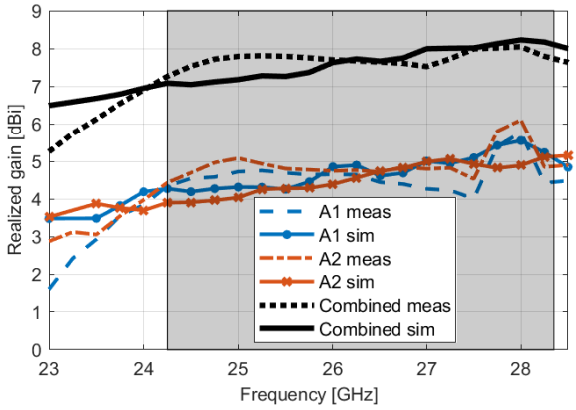

Fig. 16. Realized gain in the endfire direction ($+z$ axis) of the antenna elements separately and the in-phase combination of them.

wave modules if the whole sphere has to be covered. The most similar solution corresponds to the previous work from the authors [15] since they both have the goal of preventing the blockage caused by the metallic frame of the phones, without removing a large section of the bezel. In that design, the reduction of the main-beam blockage in the presence of a metallic bezel is achieved with two tilted layers of metal strips located at both edges of the frame. The energy impinging on the frame is coupled to the layers of metal strips, that act as parasitic radiators and the fields are added in phase in the far-field. In this paper, the horizontal currents excited on the frame by the mm-wave antenna are utilized differently. The idea is to

TABLE II
COMPARISON OF THIS PAPER WITH THE PREVIOUS WORK

	Volume [mm^3]	Antenna-frame distance [mm]	Band [GHz]	Pattern	Peak gain in band [dBi]	Num. antennas	Beam-steering	Embeddable	Gain improvement
[7]	43.6 x 7.1 x 1	N.A.	27.2-28.5	Broadside	14	8 (8 active)	$0° \sim 60°$	No	N.A.
[16]	51.3 x 7 x 4	N.A.	27.5-30	Broadside	15.6	8 (8 active)	$0° \sim 60°$	No	N.A.
[17]	17.8 x 8 x 2.5	N.A.	27-28.5	Endfire	11.7	8 (8 active)	$\pm 80°$	No	N.A.
[18]	30 x 5 x 5	N.A.	27-29.5; 36.8-40.3	Broadside	11.3; 12	5 (5 active)	$-60° \sim 0°$	No	N.A.
[14]	23 x 7 x 4	N.A.	25-30	Endfire	7	4 (4 active)	$\pm 25°$	Yes	No
[15]	30 x 8.8 x 0.64	7	24-27.5	Endfire	11	6 (4 active)	$\pm 60°$	Yes	No
This work (2 active)	**21.7 x 7.75 x 0.64**	**0.5**	**22-28.4**	**Endfire**	**8**	**4 (2 active)**	**$-40° \sim 40°$**	**Yes**	**Yes**
This work (4 active)	**21.7 x 7.75 x 0.64**	**0.5**	**22-28.4**	**Endfire**	**10.7**	**4 (4 active)**	**$-80° \sim 70°$**	**Yes**	**Yes**

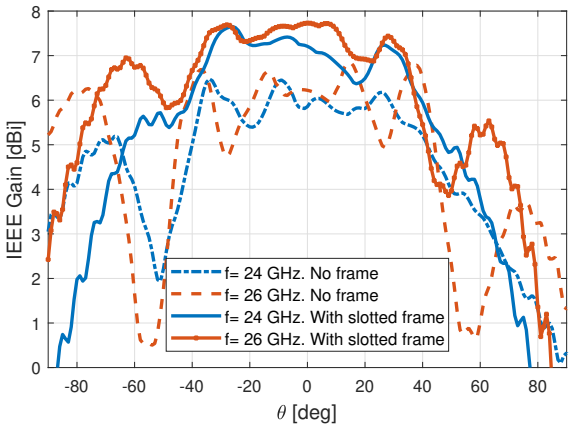

Fig. 17. Simulated beam-steering envelope comparison of the array without frame and with the slotted frame.

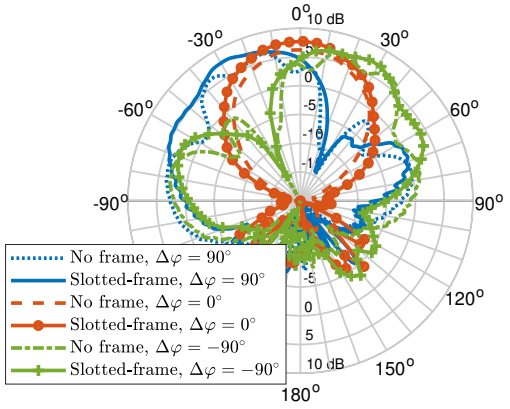

Fig. 18. Radiation pattern comparison at the $\Phi = 90°$ cut of the array without frame and with the slotted frame for three different beams at 26 GHz.

etch slots on the frame so they can be fed by these horizontal currents. This way the array aperture is enlarged and the gain increases. The design of this paper provides the lowest number of active elements with a peak realized gain of 8 dBi. The proposals in [14], [15] allow the embedding of the mm-wave array in the low-frequency metal-frame antenna, but no gain enhancement is achieved after the embedding. However, the solutions in this work are able to increase at least 1.5 dB the gain of the antenna in free-space. Comparing with [15], the distance from the top part of the mm-wave array to the bezel is considerably reduced in this paper.

VII. CONCLUSION

The method proposed in this paper to overcome the blockage of the frame to endfire 5G arrays is to etch several slots on the side of the frame where the mm-wave array is located. The slots not only reduce the obstruction but also enhance the gain of the array. A bow-tie array is designed as endfire mm-wave array, and it is embedded in the handset frame, which is used as sub-3 GHz antenna. The co-design of the two antennas is simple, with the clearance of the bow-tie array as the only constraint, imposed by the low-frequency antenna. As shown in the results, both antennas operate independently without degrading the performance of the other.

Design considerations have been studied to obtain the best performance of the array. In order to broaden the beam-steering scanning properties, the aperture of the slot array needs to be larger than the mm-wave array. The distance from the top part of the bow-tie array to the frame defines the impedance bandwidth and gain. Small distances provide wide impedance matching but with lower gain. The performance of the proposed array has been compared with its counterpart with 4 active elements and no frame. Two more active antennas can increase the gain around 0.5 dB and broaden the scanning range. The final design has been manufactured and measured. Good agreement is found between measurements and simulations. The mm-wave array is matched from 22-28.4 GHz, covering the n258 and n261 bands. Measured radiation patterns demonstrate the principle, with a gain higher than 7 dBi in the operating band. The array is able to scan in the range $-40° < \theta < 40°$. The low-frequency antenna covers the frequency bands 760-980 MHz and 1240-2870 MHz.

ACKNOWLEDGMENT

The authors would like to thank Ben Krøyer for his help in the antenna manufacturing and Kim Olesen for his assistance in the chamber set-up.

REFERENCES

[1] W. Hong, K.-H. Baek, Y. Lee, Y. Kim, and S.-T. Ko, "Study and prototyping of practically large-scale mmwave antenna systems for 5G cellular devices," *IEEE Commun. Mag.*, vol. 52, no. 9, pp. 63–69, 2014.

[2] Z. Pi and F. Khan, "An introduction to millimeter-wave mobile broadband systems," *IEEE Commun. Mag.*, vol. 49, no. 6, 2011.

[3] T. S. Rappaport, S. Sun, R. Mayzus, H. Zhao, Y. Azar, K. Wang, G. N. Wong, J. K. Schulz, M. Samimi, and F. Gutierrez, "Millimeter wave mobile communications for 5G cellular: It will work!" *IEEE Access*, vol. 1, pp. 335–349, 2013.

[4] W. Hong, K.-H. Baek, and S. Ko, "Millimeter-wave 5G antennas for smartphones: Overview and experimental demonstration," *IEEE Trans. Antennas Propag.*, vol. 65, no. 12, pp. 6250–6261, 2017.

[5] M. Stanley, Y. Huang, H. Wang, H. Zhou, A. Alieldin, and S. Joseph, "A novel mm-wave phased array antenna with 360° coverage for 5G smartphone applications," in *2017 10th UK-Europe-China Workshop on Millimetre Waves and Terahertz Technologies (UCMMT)*. IEEE, 2017, pp. 1–3.

[6] Y. Wang, H. Wang, and G. Yang, "Design of dipole beam-steering antenna array for 5G handset applications," in *2016 Progress in Electromagnetic Research Symposium (PIERS)*. IEEE, 2016, pp. 2450–2453.

[7] J. Bang and J. Choi, "A SAR reduced mm-wave beam-steerable array antenna with dual-mode operation for fully metal-covered 5G cellular handsets," *IEEE Antennas Wireless Propag. Lett.*, vol. 17, no. 6, pp. 1118–1122, 2018.

[8] R. Rodríguez-Cano, S. Zhang, and G. F. Pedersen, "Beam-steerable multi-band mm-wave bow-tie antenna array for mobile terminals," in *12th European Conference on Antennas and Propagation (EuCAP 2018)*, April 2018, pp. 1–4.

[9] R. A. Alhalabi and G. M. Rebeiz, "High-efficiency angled-dipole antennas for millimeter-wave phased array applications," *IEEE Trans. Antennas Propag.*, vol. 56, no. 10, pp. 3136–3142, 2008.

[10] S. Zhang, I. Syrytsin, and G. F. Pedersen, "Compact beam-steerable antenna array with two passive parasitic elements for 5G mobile terminals at 28 GHz," *IEEE Trans. Antennas Propag.*, vol. 66, no. 10, pp. 5193–5203, 2018.

[11] I. Syrytsin, S. Zhang, G. F. Pedersen, and A. S. Morris, "Compact quad-mode planar phased array with wideband for 5G mobile terminals," *IEEE Trans. Antennas Propag.*, vol. 66, no. 9, pp. 4648–4657, 2018.

[12] M. M. Samadi Taheri, A. Abdipour, S. Zhang, and G. F. Pedersen, "Integrated millimeter-wave wideband end-fire 5G beam steerable array and low-frequency 4G LTE antenna in mobile terminals," *IEEE Trans. Veh. Technol.*, vol. 68, no. 4, pp. 4042–4046, April 2019.

[13] R. Hussain, A. T. Alreshaid, S. K. Podilchak, and M. S. Sharawi, "Compact 4G MIMO antenna integrated with a 5G array for current and future mobile handsets," *IET Microw., Antennas Propag.*, vol. 11, no. 2, pp. 271–279, 2017.

[14] J. Kurvinen, H. Kähkönen, A. Lehtovuori, J. Ala-Laurinaho, and V. Viikari, "Co-designed mm-wave and LTE handset antennas," *IEEE Trans. Antennas Propag.*, vol. 67, no. 3, pp. 1545–1553, 2019.

[15] R. Rodriguez-Cano, S. Zhang, K. Zhao, and G. F. Pedersen, "Reduction of main beam-blockage in an integrated 5G array with a metal-frame antenna," *IEEE Trans. Antennas Propag.*, vol. 67, no. 5, pp. 3161–3170, May 2019.

[16] B. Yu, K. Yang, G. Yang *et al.*, "A novel 28 GHz beam steering array for 5G mobile device with metallic casing application," *IEEE Trans. Antennas Propag.*, vol. 66, no. 1, pp. 462–466, 2018.

[17] S. S. Kim, S. H. Kim, J. H. Bae, and Y. J. Yoon, "Switched folded slot phased array antenna for mm wave 5G mobile in metal bezel design," in *2018 IEEE International Symposium on Antennas and Propagation & USNC/URSI National Radio Science Meeting*. IEEE, 2018, pp. 239–240.

[18] Y. Wang, H.-C. Huang, and X. Jian, "Novel design of a dual-band 5G mm-wave antenna array integrated with a metal frame of a cellular phone," in *2018 Asia-Pacific Microwave Conference (APMC)*. IEEE, 2018, pp. 1582–1584.

[19] "General aspects for User Equipment (UE) Radio Frequency (RF) for NR (Release 15)," 3rd Generation Partnership Project (3GPP), Technical Report (TR) 38.817-1, 03 2019, version 15.3.0.

[20] K. Loi, S. Uysal, and M. Leong, "Design of a wideband microstrip bowtie patch antenna," *IEE Proceedings-Microwaves, Antennas and Propagation*, vol. 145, no. 2, pp. 137–140, 1998.

[21] C. Deng, Z. Xu, A. Ren, and S. V. Hum, "TCM-based bezel antenna design with small ground clearance for mobile terminals," *IEEE Trans. Antennas Propag.*, vol. 67, no. 2, pp. 745–754, 2019.

[22] A. Vasjanov and V. Barzdenas, "A review of advanced CMOS RF power amplifier architecture trends for low power 5G wireless networks," *Electronics*, vol. 7, no. 11, p. 271, 2018.

[23] N. Rostomyan, M. Özen, and P. Asbeck, "28 GHz doherty power amplifier in CMOS SOI with 28 percent back-off PAE," *IEEE Microw. Wirel. Compon. Lett.*, vol. 28, no. 5, pp. 446–448, 2018.

Rocio Rodriguez-Cano (S'17) was born in Granada (Spain) in 1993. She received the B.S. degree and MsC. in Electrical Engineering at the University of Malaga, Spain, in 2015 and 2017, respectively. She is currently pursuing a Ph.D. in antenna systems for the next generation of mobile terminals at Aalborg University, Denmark. In November 2019, she was a Visiting Ph.D. Student with the Global Big Data Technologies Centre, University of Technology Sydney, Australia. Her current research interests include antenna design for 5G communications, integration with the former generations of mobile communications, user exposure and small antennas.

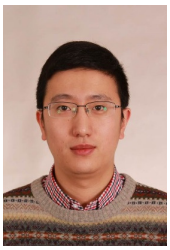

Shuai Zhang (SM'18) received the B.E. degree from the University of Electronic Science and Technology of China, Chengdu, China, in 2007 and the Ph.D. degree in electromagnetic engineering from the Royal Institute of Technology (KTH), Stockholm, Sweden, in 2013. After his Ph.D. studies, he was a Research Fellow at KTH. In April 2014, he joined Aalborg University, Denmark, where he currently works as Associate Professor. In 2010 and 2011, he was a Visiting Researcher at Lund University, Sweden and at Sony Mobile Communications AB, Sweden, respectively. He was also an external antenna specialist at Bang & Olufsen, Denmark from 2016-2017. He has coauthored over 50 articles in well-reputed international journals and over 15 (US or WO) patents. His current research interests include: mobile terminal mmwave antennas, biological effects, CubeSat antennas, Massive MIMO antenna arrays, UWB wind turbine blade deflection sensing, and RFID antennas.

Kun Zhao received the B.S. degree in Communication Engineering from Beijing University of Posts and Telecommunications (BUPT), Beijing, China in 2010, M.S. in wireless systems and Ph.D. degree in electromagnetic engineering from Royal Institute of Technology (KTH), Stockholm, Sweden, in 2012 and 2017, respectively. Currently, he is a researcher of antenna technology and standardization in the Radio Access Lab, Sony Mobile Communication AB, Lund, Sweden. He also works as an industrial post-doc at Aalborg University, Denmark. He was a visiting researcher at the Department of Electrical and Information Technology, Lund University, Sweden. His current research interests include mm-wave antenna and propagation for 5G communications, MIMO antenna systems, user body interactions, and body centric wireless communications.

Gert Frølund Pedersen (M'14) was born in 1965. He received the B.Sc. and E.E. (Hons.) degrees in electrical engineering from the College of Technology in Dublin, Dublin Institute of Technology, Dublin, Ireland, in 1991, and the M.Sc.E.E. and Ph.D. degrees from Aalborg University, Aalborg, Denmark, in 1993 and 2003, respectively. Since 1993, he has been with Aalborg University where he is a Full Professor heading the Antennas, Propagation and Millimeter-wave Systems LAB with 25 researchers. He is also the Head of the Doctoral School on wireless communication with some 40 Ph.D. students enrolled. His research interests include radio communication for mobile terminals especially small antennas, diversity systems, propagation, and biological effects. He has published more than 500 peer reviewed papers, 6 books, 12 book chapters and holds over 50 patents. He has also worked as a Consultant for developments of more than 100 antennas for mobile terminals including the first internal antenna for mobile phones in 1994 with lowest SAR, first internal triple-band antenna in 1998 with low SAR and high TRP and TIS, and lately various multiantenna systems rated as the most efficient on the market. He has worked most of the time with joint university and industry projects and have received more than 21 M$ in direct research funding. He is currently the Project Leader of the RANGE project with a total budget of over 8 M$ investigating high performance centimetre/millimetre-wave antennas for 5G mobile phones. He has been one of the pioneers in establishing over-the-air measurement systems. The measurement technique is now well established for mobile terminals with single antennas and he was chairing the various COST groups with liaison to 3GPP and CTIA for over-the-air test of MIMO terminals. He is currently involved in MIMO OTA measurement.